Microwave loss mechanisms in $Ba_{0.25}Sr_{0.75}TiO_3$ thin film varactors

A. Vorobiev, P. Rundqvist, K. Khamchane, and S. Gevorgian

Citation: Journal of Applied Physics **96**, 4642 (2004);
View online: https://doi.org/10.1063/1.1789631
View Table of Contents: http://aip.scitation.org/toc/jap/96/8
Published by the American Institute of Physics

Microwave loss mechanisms in $Ba_{0.25}Sr_{0.75}TiO_3$ thin film varactors

A. Vorobiev,[a] P. Rundqvist, and K. Khamchane
Department of Microtechnology and Nanoscience, Chalmers University of Technology, SE-41296 Gothenburg, Sweden

S. Gevorgian
Department of Microtechnology and Nanoscience, Chalmers University of Technology, SE-41296 Gothenburg, Sweden
Microwave and High Speed Electronics Research Center, Ericsson AB, 431 84 Moelndal, Sweden

(Received 23 February 2004; accepted 13 July 2004)

Parallel-plate Au(Pt)/$Ba_{0.25}Sr_{0.75}TiO_3$/(Pt)Au thin film varactors were fabricated on high resistance Si substrates and characterized at dc, rf, and microwave frequencies. In the frequency range 10–45 GHz the varactors show relatively low losses, with loss tangent less than 0.025 at 45 GHz. Due to the thick and highly conductive Pt/Au electrodes the metal losses are less than 10%. However, the loss tangent of the ferroelectric film is still three to five times higher than that in $Ba_{0.27}Sr_{0.73}TiO_3$ single crystal. The analysis of the dc field dependences of loss tangent and permittivity in a wide frequency range shows that these additional losses are mainly due to the charged defects. Extrapolation of measured low frequency (1 MHz) loss tangents to the microwave region using the power law $\omega^{1/3}$ is in good agreement with experiment. The dc current through the varactor is found to be controlled by Schottky emission and Poole-Frenkel mechanisms depending on the polarity. The Poole-Frenkel mode is associated with field enhanced thermal excitation of charge carriers from internal traps. The trap activation energy (about 0.15 eV) determined from the Poole-Frenkel mode agrees well with the energy level of the oxygen vacancy. We assume that the oxygen vacancies within the grain boundaries of the ferroelectric film act as charged defects and cause additional (extrinsic) microwave losses. The possible correlation between the film's internal strains and density of the oxygen vacancies are discussed. The knowledge of the extrinsic loss mechanism and corresponding microstructure defects is useful in optimization of the varactor design, deposition, annealing process, and further improvement of the varactor performance. © *2004 American Institute of Physics*. [DOI: 10.1063/1.1789631]

I. INTRODUCTION

Parallel-plate $Ba_xSr_{1-x}TiO_3$ (BST) thin film varactors have been considered for applications in tunable microwave devices.[1–3] Recently it was shown that the total losses of these varactors may be substantially reduced by using thick Au bottom electrodes.[4,5] However, due to the defects in the ferroelectric films the dielectric losses remain substantially higher than those in single crystals.[6] The dominant extrinsic microwave losses in ferroelectric films may be due to the charged defects, local polar regions, and grain boundaries. The field and frequency dependent models of the extrinsic losses and permittivity were developed by Tagantsev and Vendik.[6–8] By using these models and analyzing the experimental field and frequency dependences of the permittivity and loss tangent, the dominant loss mechanisms can be identified. The identification of the dominant loss mechanisms and their correlation with the defects may help to develop methods of improving the ferroelectric film microstructure and thereby reduce the microwave losses down to the fundamental limit.

Charged defects are usually associated with oxygen vacancies within nonstoichiometric grain boundaries.[9] The local polar regions are associated with the planar (grain boundaries), linear (dislocations), and/or point (vacancies and/or substituted atoms) defects.[6] These defects may be detected directly using a detailed microstructural analysis of the films and interfaces. However, the microstructural analysis is a rather complex process requiring special and time-consuming sample preparations (cross section, layer by layer etching, etc.). The preparation procedure may often affect the sample properties (for example, change the stoichiometry and/or induce impurities) and lead to misinterpretation of the results.

In this work we use an alternative approach to detect and identify the defects by measuring a nonlinear dc current through a ferroelectric film. A number of publications have been devoted to this subject.[10–12] The most probable mechanisms controlling the nonlinear dc current through perovskite films are: Schottky-emission, Pool-Frenkel emission, and space-charge limited current (SCLC). Usually, the Schottky mechanism is attributed to the current through the barrier at the film-electrode interface, while the Pool-Frenkel and SCLS mechanisms are attributed to the defects at grain boundaries.[13] The analysis of the field and temperature dependences of the dc current allow for the extraction of the defect parameters, i.e., the height of the energy barrier at

[a]Author to whom correspondence should be addressed; Permanent address: Institute for physics of microstructures, GSP-105, Nizhny Novgorod, 603950 Russia; electronic mail: andrei.vorobyev@mc2.chalmers.se

ferroelectric film/electrode interfaces, and/or the activation energy of the internal traps.[11,14] These parameters can be used to identify the type of defects.

In this work, the dominant extrinsic microwave loss mechanism in $Ba_{0.25}Sr_{0.75}TiO_3$ films is identified via experimental field and frequency dielectric spectroscopy, while the type of the defects behind this loss mechanism is identified through the analysis of the dc conduction mechanisms.

II. DIELECTRIC LOSSES IN FERROELECTRICS

$Ba_{0.25}Sr_{0.75}TiO_3$ is ferroelectric of displacive type in paraelectric state at room temperature (the phase transition point is 125 K).[15] The theory of dielectric losses for this type of ferroelectrics was developed and summarized by Tagantsev and Vendik.[6,7] For a ferroelectric film both the intrinsic (fundamental phonon loss mechanisms) and the extrinsic losses (due to the defects) need to be considered. The models of the dominant loss mechanisms in the ferroelectric films will be discussed in this section, to be used in the further analysis and interpretation of experimental results.

A. Intrinsic losses

The origin of the fundamental losses is the ac field interaction with the phonons. In centrosymmetric crystals (e.g., $Ba_{0.25}Sr_{0.75}TiO_3$ without dc field) the three- and four-quantum mechanisms control the intrinsic losses. For the frequencies ω less than the damping of phonons Γ (for $SrTiO_3$ $\omega \leqslant 100$ GHz), the phonon transport theory gives the functional dependence of the loss tangent

$$\tan \delta_{ph} \propto \omega T^2 \varepsilon^{3/2}, \tag{1}$$

where ω is the angular frequency, T is temperature, and ε is the real part of relative dielectric permittivity.[6]

In noncentrosymmetric crystals (e.g., $Ba_{0.25}Sr_{0.75}TiO_3$ under dc field E) the quasi-Debye mechanism contributes to the total intrinsic losses.[16] For frequencies $\omega \leqslant \Gamma$ this contribution is presented as[6]

$$\tan \delta_{QD}(E) = A\omega I(E) n_\varepsilon, \tag{2}$$

where A is a fitting parameter. In the limit of small relative tuneability (small fields E) $n_\varepsilon = \varepsilon(0)/\varepsilon(E)$ the function $I(E) \rightarrow 1$. For higher fields, the $\tan \delta_{QD}$ versus E dependence deviates from this simple law and appears to be different for different materials. The simulation[6] for a $Ba_{0.6}Sr_{0.4}TiO_3$ crystal at 1 GHz and $E > 200$ kV/cm (the fields applicable in our case) gives almost flat $\tan \delta_{QD}(E)$ dependence with $\tan \delta_{QD} \approx 6 \times 10^{-4}$.

B. Extrinsic losses

In displacive paraelectrics the losses due to charged defects are associated with electrostriction. The electrostriction about the charged defect excites acoustic vibrations in the medium, which tends to dissipate the energy of the microwave field. It has been shown[6] that the losses due to charged defects are characterized by a nearly linear frequency dependent loss tangent, $\tan \delta_{ch} \sim \varepsilon\omega$. However, experimental results indicate that the loss tangent-frequency behavior better corresponds to

$$\tan \delta_{ch} = A(E)\omega^{1/3}, \tag{3}$$

where $A(E)$ is a fitting parameter.[17] An essential feature of this mechanism is that the loss tangent is proportional to the permittivity, and it decreases with the increased dc field, in the same way as the permittivity does.[6,17]

According to the universal relaxation law,[8] the real ε and imaginary ε_{im} parts of the permittivity have the same frequency dependence (ω^{n-1}, where $0 < n < 1$) and therefore the loss tangent is frequency independent ($\tan \delta = \varepsilon_{im}/\varepsilon$).

The local polar regions transform microwave field oscillations into acoustic oscillations.[7] The theory of the local polar regions is not completely developed. However, it is expected that the contribution of the "defect-induced" quasi-Debye mechanism[6] should be strongly permittivity dependent, $\tan \delta_{dQD} \propto \varepsilon^{4.5-d}$, where $d=2$ for planar defects like grain boundaries, $d=1$ for linear defects, and $d=0$ for point defects.

III. EXPERIMENT

Platinized silicon ($Pt/TiO_2/SiO_2/Si$) with resistivity $\rho_{Si} = 5$ kΩ cm was used as the substrate. Pt(50 nm)/Au(0.5 μm) bottom electrode films were deposited by e-beam evaporation at room temperature, followed by growth of 300 nm thick BST films using a KrF excimer laser ($\lambda = 248$ nm, $\tau = 30$ ns) operating at 10 Hz with an energy density of 1.5 J cm^{-2} to ablate the $Ba_{0.25}Sr_{0.75}TiO_x$ target. The substrate temperature was maintained at 650 °C and oxygen pressure at 0.4 mbar. After deposition the samples were cooled down to room temperature at 950 mbar oxygen pressure. To keep the parallel-plate structure symmetric, the Au(0.5 μm)/Pt(50 nm) top electrodes were deposited on BST by e-beam evaporation at room temperature.

A lift-off process was used to pattern the top electrodes. The top electrodes were patterned as central circular patches surrounded by cocentric electrodes. Test structures with radii of the center patch $a = a_1 = 4$ μm and $a = a_2 = 15$ μm were used in the experiments. The total capacitance measured between the center patch and surrounding cocentric electrode is $C = (C_f C_{out})/(C_f + C_{out})$, where C_f is the capacitance between the center patch and bottom plate, and C_{out} is the capacitance between the top outer electrode and bottom plate. Typically, $C_{out} \gg C_f$ and the top outer electrode provides effective dc and microwave "connection" to the bottom plate. In both cases the internal diameter of the cocentric outer electrode is 100 μm.

The thickness d_f of the BST films was measured using a Tencor Alfastep 500 profilometer at the step formed by the deposition through a shadow mask. An image of the BST film surface was obtained using an atomic force microscope (AFM) Dimension 3100 SPM operating in tapping mode. The capacitance-voltage (C-V) dependences of the varactors were measured using a HP 4285A LCR-meter at 1 MHz and at different rf voltage levels (0.3, 1.0, and 2.0 V_{rms}). In measurements, the dc bias was reversed periodically (one cycle) to record possible hysteresis effects in C-V performance. The current-voltage (I-V) dependences were measured using a HP4145B semiconductor parameter analyzer.

The microwave parameters of the varactors were measured using a HP 8510C vector network analyzer and ground-signal-ground microprobes in the frequency range of 100 MHz–45 GHz. Two different calibrations in the frequency ranges below and above 10 GHz were used to increase the number of experimental points. The complex input impedance of the varactor was extracted from one port reflection measurements. The capacitance C and the loss tangent $\tan\delta$ were computed from the complex impedance $Z=R+jX, C=-I/\omega(X-\omega L_{\text{ser}}), \tan\delta=-R/X$, where L_{ser} is the series (parasitic) inductance of the electrodes. In our experiments $L_{\text{ser}}\approx 1.5\times 10^{-11}$ H.

We analyzed the contribution of the electrode series resistance and inductance to the calculated $\tan\delta$. The series resistance consists of the microprobe contact resistances R_{cont} and the resistance of the Au electrodes R_M: $R_{\text{ser}}=R_{\text{cont}}+R_M$. Typically, the gold contact resistance is less than 0.01 Ω.[18] The resistance of the electrodes is $R_M=R_{\text{center}}+R_{\text{ring}}$, where

$$R_{\text{center}}\cong\frac{R_S}{8\pi} \tag{4a}$$

and

$$R_{\text{ring}}=\frac{R_S}{2\pi}\ln\left(\frac{a}{b}\right). \tag{4b}$$

R_s is the surface resistance of the Au layer and b is the distance between signal and ground probe pins.[19] As the skin depth δ is less than the thickness of the Au electrodes (0.5 μm) above 20 GHz, δ is used to calculate R_s. By comparing R_{ser} with the real part of the measured impedance R, we found that the contribution of the series resistance to the losses is less than 10% over the whole frequency range. Comparing the calculated ωL_{ser} with the imaginary part of the measured impedance X, we found that the contribution of the series inductance to the calculated $\tan\delta$ ($\tan\delta=-R/X$) is less than 10% over the whole frequency range. The series resistance and inductance only give a minor contribution to the calculated $\tan\delta$ and may therefore be neglected. At lower frequencies, especially below 5–10 GHz, the thickness of the bottom electrode is smaller than the skin depth, and the ac field penetrates into the silicon substrate causing extra losses associated with the free carrier absorption in silicon.

IV. RESULTS AND DISCUSSIONS

A. Permittivity and microwave losses

1. Permittivity of the film

Figure 1 shows the typical dc bias dependences of the capacitance C and $\tan\delta$ of a varactor at 1.0 MHz and 0.3 V_{rms} rf voltage. The C-V curve has no "butterfly" shape (i.e., with two peaks in voltage dependence of capacitance) indicating that the BST film is in a paraelectric state. The tuneability of the capacitance at 20 V is more than 40%. Higher tuneability is expected at higher dc bias fields. The $\tan\delta$ is less than 0.0045 at 0 V and decreases with the dc field.

Figure 2(a) shows the capacitance at 0 and 20 V dc bias versus frequency. The capacitance is relatively frequency independent in the range of 100 MHz–45 GHz, which indicates that permittivity is determined mainly by the soft phonon mode contribution[6,20] with a resonant frequency ~3 THz.[20] The tuneability of the capacitance at 20 V bias is about 40% over the whole frequency range. The permittivities calculated from the simple parallel-plate model

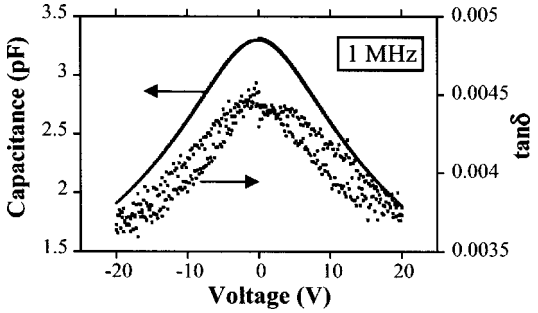

FIG. 1. Capacitance-voltage and loss tangent-voltage dependences of a varactor at 1.0 MHz and 0.3 V_{rms} rf voltage level.

$$\varepsilon = Cd_f/(\varepsilon_0\pi a^2) \tag{5}$$

are 158 and 169 for test structures with radii $a=a_1=4$ μm and $a=a_2=15$ μm, respectively ($\varepsilon_0=8.85\times 10^{-12}$ F/m is the dielectric constant of free space). The difference in measured ε is less than 6% and is within the accuracy of measurements. Thus, as a first approximation, the contribution of C_{out} in the reduction of permittivity calculated using Eq. (5) can be neglected.

It is customary to compare the permittivity of the thin films with the permittivity of single crystals. The permittivity of single crystal $Ba_{0.27}Sr_{0.73}TiO_3$ estimated using the Curie-Weiss law $\varepsilon_b=C_{\text{CW}}/(T-T_C)\approx 510$, where $C_{\text{CW}}\approx 9\times 10^4$ K is the Curie-Weiss constant and $T_C\approx 125$ K.[15,21] The mea-

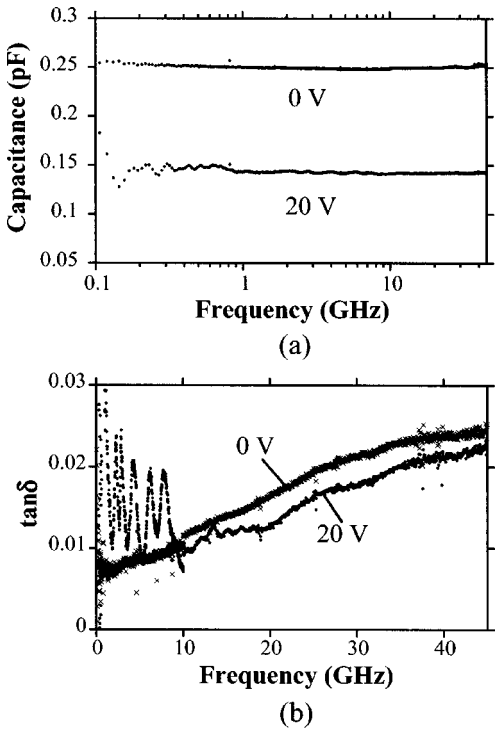

FIG. 2. Frequency dependences of capacitance (a) and loss tangent (b) of varactor at $V=0$ and 20 V of dc bias.

sured permittivity, which is calculated using Eq. (5), is substantially smaller than ε_b. One may expect a reduction of the film permittivity due to the defects in the film, at the interfaces, and due to the strains (both internal and interfacial).[22] More often the interfacial "dead layers" are considered as the explanation for the apparent low permittivity. The nature of the dead layers is not completely understood.[23] It is usually associated with the interdiffusion, chemical reactions, contamination, and/or structural defects at the interfaces.[23–27] These processes are more pronounced at the bottom electrode/BST film interface since the growth temperature of the BST film is much higher than the deposition temperature of the top electrode. Simple estimations show that the thickness of the dead layer in our varactor may be about $d_d \approx 30$ nm, assuming the permittivity of the BST film $\varepsilon \approx 500$, and the permittivity of the dead layer about $\varepsilon_d \approx 20$.

2. Tuneability

In general, the effect of interfacial layers on the performance of the parallel-plate capacitors is distractive in several ways. The interfacial layer is connected in series with the bulk of the ferroelectric film and reduces the capacitance and the apparent permittivity, as mentioned previously. Additionally, it reduces the tuneability of the varactor. In an ideal case, where there are no interfacial dead layers ($\varepsilon = \varepsilon_b$), the tuneability of the film permittivity and the tuneability of the capacitance C_b (ignoring fringing field capacitance) are identical:

$$T_\varepsilon(V) = T_c(V) = \frac{\varepsilon_b(0) - \varepsilon_b(V)}{\varepsilon_b(0)} = \frac{C_b(0) - C_b(V)}{C_b(0)}. \tag{6}$$

In the presence of two identical interfacial layers (capacitances C_d) the total capacitance of the parallel-plate capacitor is $C(V) = [2C_d C_b(V)]/[2C_d + C_b(V)]$, then the tuneability of the capacitor is

$$T(V) = \frac{C(0) - C(V)}{C(0)} = \frac{C_b(0) - K_d(V)C_b(V)}{C_b(0)}, \tag{7}$$

where

$$K_d(V) = \frac{2C_d + C_b(0)}{2C_d + C_b(V)}.$$

It is clear that $K_d(V) > 1$, which means a reduced tuneability $T(V) < T_\varepsilon(V)$. It is possible to calculate the tuneability of the ideal varactor (without dead layers). Using the measured tuneability $T(V) = 0.4$ and assuming $\varepsilon_b = 500$, $\varepsilon_d = 20$, and $d_d = 30$ nm, one obtains $T_\varepsilon(V) \approx 0.7$. This reduction of tuneability demonstrates the destructive influence of dead layers on the performance of a varactor. Note also that a part of the applied dc field drops over the interfacial layers (capacitances), which are not tuneable and have lower permittivity.[28] The reduction of the tuneability is seen in Fig. 1, where our 0.3 μm thick film does not show trends of saturation even at voltages up to 20 V ($E = V/d \approx 700$ kV/cm), while the saturation in the bulk $SrTiO_3$ (STO) appears below 10 kV/cm. Additionally, the decreased tuneability will limit the varactor as a nonlinear device (i.e., mixer or multiplier). The detailed studies of the dead layer properties and their influence on our varactor performance will be published in a separate paper.

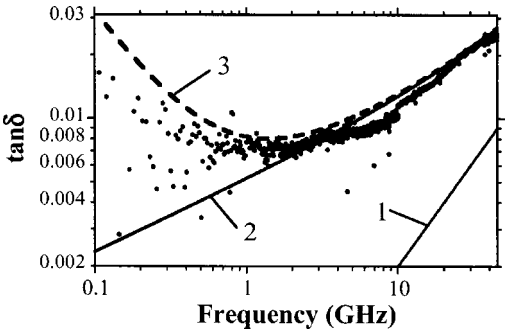

FIG. 3. The loss tangent of varactor vs frequency at 0 V dc bias. Shown are also loss tangents of: $Ba_{0.27}Sr_{0.73}TiO_3$ single crystal — 1, BST film with charged defects — 2, BST film with charged defects and Si substrate in sum — 3.

3. Microwave losses

The interfacial dead layers may cause extra losses due to the Maxwell-Vagner relaxation.[29] However, in our experiments no capacitance (permittivity) dispersion is observed in the frequency range of 100 MHz–45 GHz [Fig. 2(a)], which indicates that this type of relaxation plays a minor role in the total dielectric response (apparent permittivity and losses).

Figure 2(b) shows the frequency dependences of tan δ at 0 and 20 V dc bias. The glitches at 10 GHz are due to the uncertainty of the calibrations. The loss tangent increases with frequency up to 0.025 at 45 GHz [Fig. 2(b)]. The peaks in loss tangent in the frequency range of 1–20 GHz under applied dc voltage are due to the resonant conversion of the microwave power into acoustic waves.[17] Away from the resonant peaks, the loss tangent decreases with the dc field [Fig. 2(b)] in accordance with the low frequency measurements (Fig. 1).

To estimate the extrinsic losses in the BST film, we compare the measured losses of the varactor with those in a single crystal of the same composition having intrinsic losses only. For a $Ba_{0.27}Sr_{0.73}TiO_3$ single crystal tan $\delta \cong 0.002$ at 10 GHz and room temperature,[15] while the measured loss tangent of our BST film at 10 GHz is about five times larger. The frequency dependence of the loss tangent for a single crystal $Ba_{0.27}Sr_{0.73}TiO_3$ is shown in Fig. 3 (curve 1), where a linear frequency dependence (1) is assumed. This dependence gives only the intrinsic losses in the material associated with multiphonon scattering of the soft ferroelectric mode. Thus it is clear that the extrinsic losses dominate in our BST films. Below we analyze the contributions of extrinsic losses due to different mechanisms.

As indicated previously, the universal relaxation law predicts frequency independent loss tangent. No such dependence is observed in our experiments [Fig. 2(b)]. Hence, this mechanism does not contribute significantly to the total loss balance. This result is expected from the film structure in our parallel-plate capacitor. The films have columnar-granular structure with no grains or grain boundaries within individual columns. Hence, in the parallel-plate capacitor the electric field lines do not cross the grain boundaries.

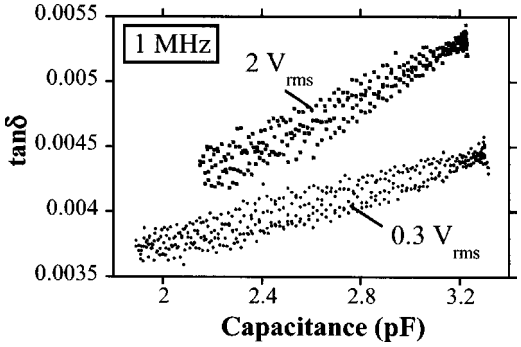

FIG. 4. Loss tangent of varactor vs capacitance at 1 MHz and different rf voltage levels (0.3 V_{rms} and 2.0 V_{rms}). The data are taken from capacitance—voltage and loss tangent-voltage measurements.

The fundamental losses (1) at 1 MHz are only $\tan \delta_{ph} \approx 2\times10^{-7}$ and may thereby be neglected (Fig. 1). The loss tangents associated with the charged defects and the local polar regions are proportional to the frequency.[6] To distinguish between these two mechanisms we analyze the relationship between the loss tangent and permittivity. Figure 4 shows the capacitance dependences of $\tan \delta$ obtained from the loss tangent — voltage, and capacitance — voltage measurements at 1.0 MHz (Fig. 1) using different rf voltages (0.3 and 2 V_{rms}). The rf voltage dependence of the dielectric properties is due to ferroelectric nonlinearity. The loss tangent dependences shown in Fig. 4 may be described as

$$\tan \delta^{1\ \mathrm{MHz}} = \tan \delta_{Si} + \tan \delta_{ch}. \tag{8}$$

The term $\tan \delta_{Si}$, associated with the losses in Si, is independent of the dc field. It appears only at low frequencies and will be discussed below. The capacitance dependence of $\tan \delta_{ch}$ (Fig. 4) is rather linear ($\tan \delta_{ch} \propto \varepsilon$) and may be associated with charged defects.[6,17] Any losses due to local polar regions would reveal stronger ε dependence,[6] indicating that the contribution of this mechanism to the total losses is small. In addition, the absence of hysteresis in the *C-V* curve (Fig. 1) indicates that regions with residual ferroelectric polarization play a minor role in the dielectric response of our BST films at 1.0 MHz. Similar linear dependences $\tan \delta_{ch} \propto \varepsilon$ have been observed at radio frequencies (10 kHz) (Ref. 30) and microwave frequencies (2 GHz) (Ref. 31) in STO thin films deposited by laser ablation and rf magnetron sputtering, respectively.

At low frequencies, especially below 5–10 GHz, the thickness of the bottom Au electrode is considerably smaller than the skin depth (0.5 μm at about 20 GHz). This leads to a substantial amount of electromagnetic field penetrating into the silicon substrate, contributing to the total loss due to the free carrier absorption.[32] This contribution is maximum near the dielectric relaxation frequency $f_{dr}=1/(2\pi\tau_{Si}) = 1/(2\pi\varepsilon_{Si}\varepsilon_0\rho_{Si})$, where τ_{Si} is the relaxation time and ε_{Si} is the dielectric permittivity of silicon. In our case $\rho_{Si} = 5\ \mathrm{k\Omega\ cm}$ and $f_{dr}=30$ MHz. According to the simple Drude model,[33] in the frequency range $f \gg f_{dr}$ the loss tangent may be given as

$$\tan \delta_{Si} = K\frac{f_{dr}}{f}, \tag{9}$$

where the coefficient $K=0.1$ takes the screening of the ac field by the bottom metal electrode into account. This inverse frequency dependence shows that the losses associated with the silicon substrate may be ignored at frequencies higher than 2 GHz (Fig. 3).

Additional losses at lower frequencies may be associated with domain related ferroelectric relaxation.[34] However, no polarization (polarization versus field) is observed in our experiments. The low frequency (1.0 MHz) *C-V* dependence (Fig. 1) also indicates that the films are in paraelectric phase, since the *C-V* dependence has no butterfly shape. Nevertheless, some local ferroelectric domains are still possible in the paraelectric matrix. Local domains have been observed both in bulk single crystal STO and thin BST films by confocal scanning optical microscopy.[35] The presence of such domains should cause the changes in the real part of the permittivity also, as it is predicted from Kramers-Kroning relationship. However, no frequency dependence is observed in the measured capacitance (real part of the permittivity) [Fig. 2(a)], so any local domains play a minor role in our films. The increase of the loss tangent with decreasing frequency below 2 GHz cannot be explained by domain wall relaxation.

The frequency dependence of the total losses in the microwave region may be calculated from the low frequency measurements (8) using the linear permittivity dependence $\tan \delta_{ch} \sim \varepsilon$.[6,17] The $\tan \delta_{ch}$ at 0 V dc bias and different rf voltages is calculated from Eq. (8) using $\tan \delta_{Si}$ obtained from Fig. 4 at the limit $C \to 0$. Then using $\tan \delta_{ch}$ at different rf voltages (0.3, 1.0, and 2.0 V_{rms}) and extrapolating to 0 V_{rms} we estimate $\tan \delta_{ch} \approx 5\times10^{-4}$ at 0 V dc bias and 0 V_{rms}. Using this value and $\omega^{1/3}$ power law (3) we obtain the frequency dependence of $\tan \delta_{ch}$. In the microwave region ($\tan \delta_{Si} \approx 0$ since the field does not penetrate to the Si substrate) the loss tangent of the BST film may be characterized as

$$\tan \delta_{film} = \tan \delta_{ch} + \tan \delta_{ph}. \tag{10}$$

The calculated frequency dependence of $\tan \delta_{film}$ is shown in Fig. 3 (curve 2). It can be seen that at frequencies higher than 2 GHz, $\tan \delta_{film}$ agrees well with the experimental data.

Finally, the total losses of the varactor at 0 V dc field are

$$\tan \delta = \tan \delta_{Si} + \tan \delta_{ch} + \tan \delta_{ph}. \tag{11}$$

The calculated frequency dependence of $\tan \delta$ (Fig. 3, curve 3) agrees well with the experiment over the studied frequency range. Thus we conclude that at frequencies above 2 GHz and 0 V dc field the losses due to the charged defects are dominant and described as

$$\tan \delta_{ch} \propto \varepsilon\omega^{1/3}. \tag{12}$$

Under the dc field in the microwave region [away from the resonant absorption, i.e., $f > 10$ GHz, Fig. 2(b)] the intrinsic quasi-Debye mechanism starts to contribute to the total loss balance due to a linear frequency dependence (2). The dc field dependence of $\tan \delta_{QD}(E)$ is rather complex.[6] At low fields the model predicts increased $\tan \delta_{QD}$ with in-

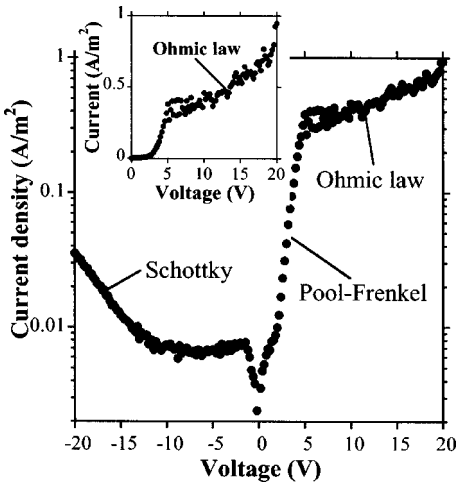

FIG. 5. The modulus of current density through BST varactor vs applied dc voltage. Insert shows the positive polarity current on the linear scales.

creased field. However, in our case the fields are rather high, which results in higher tan δ_{QD} with an almost flat field dependence. This explains the fact that the relative tuneability of the loss tangent $n_{tan}=\tan\delta(0\ \mathrm{V})/\tan\delta(20\ \mathrm{V})\approx 1.2$ is less than the relative tuneability of permittivity $n_{\varepsilon}=\varepsilon(0\ \mathrm{V})/\varepsilon(20\ \mathrm{V})\approx 1.7$ (Fig. 2).

In the next sections we identify oxygen vacancies as internal charged defects. They act as traps for charge carriers and cause extrinsic microwave losses.

B. Conduction mechanisms

Figure 5 shows the modulus of current density through the BST varactor versus applied dc voltage, i.e., the potential difference between top and bottom electrodes. It can be seen that the current is controlled by different mechanisms depending on the electrical field and the polarity. Careful examination shows that the most probable mechanisms controlling the nonlinear dc current through perovskite films are:[10–12] Schottky emission, Pool-Frenkel emission, and SCLC.

The SCLC is characterized by the current density-field relationship $J\propto E^2$, which in double log format is a straight line with a slope of 2.[36] This is not observed in our case. Hence, the *I-V* dependence (Fig. 5) cannot be explained by SCLC conduction.

The Schottky emission current density is given by

$$J_{SE}\propto \exp\left[-\frac{q}{kT}\left(\phi_{SE}-\sqrt{\frac{qE}{4\pi\varepsilon\varepsilon_0}}\right)\right], \tag{13}$$

where q is the electronic charge, k is Boltzmann's constant, and ϕ_{SE} is the barrier height.[36] The parameter $\beta_{SE}=(q/kT)\sqrt{(q/4\pi\varepsilon\varepsilon_0)}$ characterizes the slope of the straight line of $\log_{10} J_{SE}$ plotted versus $E^{1/2}$. Using the optical dielectric constant $\varepsilon_{opt}=\varepsilon=3.4$ (which is the square of the refraction index $n=1.85$),[10] β_{SE} is calculated to be $0.79\times10^{-3}\ \mathrm{C\,J^{-1}\,V^{1/2}}$. The measured slope [Fig. 6(a)] is about $0.89\times10^{-3}\ \mathrm{C\,J^{-1}\,V^{1/2}}$ and is very close to the calculated β_{SE} value. Thus, the current under negative bias is controlled by Schottky emission through the interfacial electrode/ferroelectric barrier. In our case, according to the energy band diagram of Pt/BST/Pt structure,[11,37] this corresponds to the ferroelectric/top electrode interface.

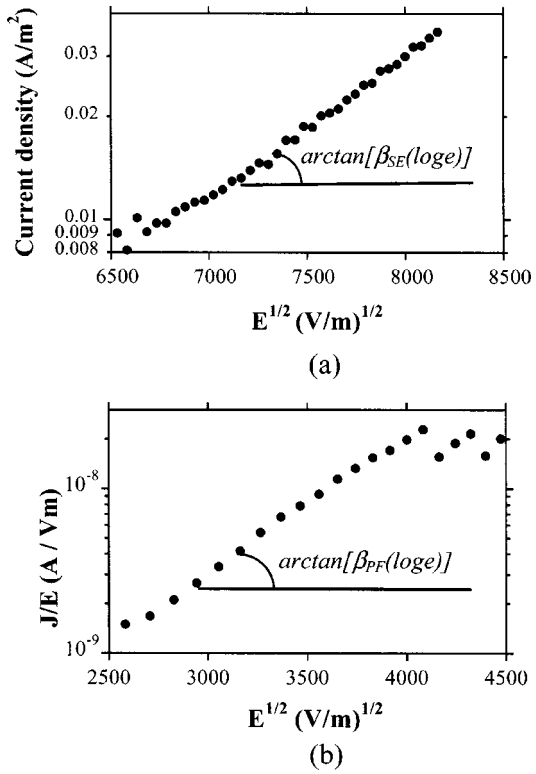

FIG. 6. The negative nonlinear current regime (Schottky mode) plotted as current density vs square root of the field $E^{1/2}$ (a) and the positive nonlinear current regime (Pool-Frenkel mode) plotted as current density-field ratio J/E vs square root of field $E^{1/2}$ (b).

The fact that the current is practically constant at smaller negative fields (Fig. 5) has a simple explanation. At low fields, the speed of the thermionic generation of charge carriers is less than the rate of the carrier transfer through the dielectric, while the field lowering of the Schottky barrier is too small to result in injection of a substantial number of carriers. Therefore the carrier density is determined mainly by the thermionic generation and is independent of the applied field (Fig. 5).

The positive branch of the *I-V* curve does not fit the β_{SE} slope and, hence, is not controlled by the Schottky barrier (Fig. 5). This can be explained by the fact that the interface at the bottom electrode is fuzzy due to Au/Pt-BST interdiffusion during growth of the ferroelectric film. In this case a bulk limited conduction mechanism can be dominating. Many experimental results show that thin dielectric films are subjected to the bulk controlled Pool-Frenkel conduction associated with field enhanced thermal excitation of charge carriers from internal traps.[10,11] The Pool-Frenkel current density is given by[36]

$$J_{PF}\propto E\exp\left[-\frac{q}{kT}\left(\phi_{PF}-\sqrt{\frac{qE}{\pi\varepsilon\varepsilon_0}}\right)\right], \tag{14}$$

where ϕ_{PF} is the barrier height. The parameter $\beta_{PF}=(q/kT)\sqrt{(q/\pi\varepsilon\varepsilon_0)}$ characterizes the slope of the straight line in the $\log_{10}(J/E)$ versus $E^{1/2}$ plot. We calculated β_{PF}

$=1.57\times10^{-3}$ C J^{-1} V$^{1/2}$, again using the optical permittivity $\varepsilon_{opt}=\varepsilon=3.4$. The measured slope [Fig. 6(b)] is about 1.66×10^{-3} C J^{-1} V$^{1/2}$ which is very close to the calculated β_{PF}. Hence, the positive current branch is controlled by the Pool-Frenkel (trapping/detrapping) mechanism, indicating that the charged defects act as internal traps. We suggest that in our BST films the oxygen vacancies act as internal traps causing Pool-Frenkel conduction, and the microwave losses. More about oxygen vacancies as structural defects is presented in the following section.

C. Oxygen vacancies

The Pool-Frenkel current regime (Fig. 5) is followed by the Ohmic law, which may be explained by field lowering of the trap barriers.[13] The resistivity estimated from the Ohmic law is $\rho\approx10^{10}$ Ω cm, the same as in good quality single crystals, where $\rho\geqslant10^{9}$ Ω cm.[38] The resistivity corresponding to the transition point (5 V) between Pool-Frenkel and Ohmic law is used to calculate the height of the trap barriers ϕ_{PF}. We assume that at the transition point 5 V (Fig. 5) the trap barriers are smoothed down by the external field, and according to Eq. (14), the following condition is fulfilled:

$$\phi_{PF}=\sqrt{\frac{qE}{\pi\varepsilon\varepsilon_0}}. \tag{15}$$

The height of the trap barriers calculated from Eq. (15) is $\phi_{PF}\approx0.16$ eV, which is in good agreement with the activation energy of 0.15 eV found from the photocapacitance measurements in the vacuum-reduced bulk STO.[39] Hence, this should be associated with the oxygen vacancies. In other words, the charged defects responsible for microwave losses and carrier transport in our BST films are associated with the oxygen vacancies. Oxygen vacancies are in fact an inherent intrinsic defect of the BST material.[40] They are located within the nonstoichiometric grain boundaries.[13] It was shown, using multiple-scattering analysis of spatially resolved electron-energy-loss spectra, that the boundary between crystalline blocks in STO carries a certain amount of oxygen vacancies, which form a surface charge on the boundary.[41] This observation is in agreement with thermodynamic predictions.[42] A model of the influence of the built-in field produced by the charged grain boundaries on the dielectric response of the ferroelectrics has been developed.[9] The volume density of single-ionized oxygen atoms may be found using a simple estimation $n=\sigma/(ql)$, where σ is the interfacial charge density at the grain boundaries and l is the size of the crystalline block.[9] The theoretical estimation for ceramics (Ba, Sr) TiO_3 showed that in the case of two-dimensional charged defects $\sigma\approx0.5$ C/m^2.[9] From the AFM image of our BST film (Fig. 7) the average size of the crystalline blocks is $l\approx0.1$ μm, resulting in $n\approx3\times10^{19}$ cm^{-3}, which is ≈0.05% of the oxygen volume concentration.

The relationship $n=\sigma/(ql)$ shows that by increasing the sizes of the crystalline blocks one can reduce the density of the oxygen vacancies and hence, the extrinsic microwave losses. Additionally, the reduction of oxygen vacancy concentration in the BST films is possible by optimization of the deposition conditions (deposition temperature,[43] pressure,[43,44] laser spot size on the target,[45] etc.), and/or by postdeposition annealing in oxygen atmosphere.[46,47]

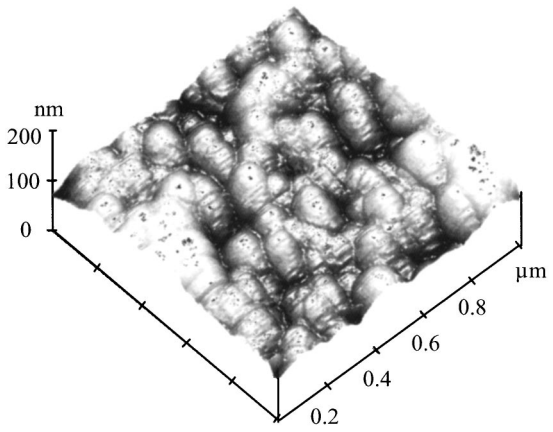

FIG. 7. An AFM image of BST film surface.

However, the reduction of the oxygen vacancies is a complex problem also associated with induced strains. In addition to the effects on the microwave losses discussed above, the oxygen vacancies also cause internal strains in the films. These strains are in equilibrium with the interfacial strains. The interfacial strains are associated with the thermal expansion coefficient mismatch and lattice mismatch between the ferroelectric film and substrate,[48,49] and other interfacing layers/films.[50] Under the complex action of these strains, the ferroelectric film is in thermodynamic equilibrium. This equilibrium sustains a certain density of oxygen vacancies, meaning that no more oxygen can be "pumped" into the film regardless of how hard we try to optimize the deposition process. This may indicate that attempts to completely or partly eliminate oxygen vacancies by monitoring only oxygen concentration may not be successful since the film will try to maintain a certain density of oxygen vacancies, i.e., the thermodynamic equilibrium. The comprehensive theoretical[51,52] and experimental[22,48] study of interfacial strains indicates that the successful reduction of the oxygen vacancies requires a careful selection of the substrates, i.e., interfacing with the film layers allowing controllable monitoring of the oxygen concentration in the film.

V. CONCLUSIONS

The dielectric losses in a $Ba_{0.25}Sr_{0.75}TiO_3$ thin film of a silicon substrate integrated parallel-plate varactor in the frequency range of 2 GHz–45 GHz (tan $\delta\approx0.025$ at 45 GHz) are mainly due to charged defects, and are described as tan $\delta_{ch}\propto\varepsilon\omega^{1/3}$. The fundamental phonon losses are several times lower (tan $\delta_{ph}\approx0.009$ at 45 GHz). Extra losses (tan $\delta\approx0.005$ at 1 MHz) at lower frequencies are due to the penetration of the ac field in the silicon substrate and absorption of the ac field power by free charge carriers. The metal losses in the electrodes are negligible over the studied frequency range because of thick Au/Pt electrodes. Extrapolation of the low frequency extrinsic loss tangents to the microwave region using the $\omega^{1/3}$ power law gives good agreement with experimental data.

Oxygen vacancies within the grain boundaries of the BST film act as charge carrier traps. The height of trap barriers, calculated from *I-V* measurements, is $\phi_{PF} \approx 0.16$ eV, which agrees well with the activation energy of the oxygen vacancies (0.15 eV).[39] The charge carrier transport in the bulk of the ferroelectric film and the extrinsic microwave losses are associated with these oxygen vacancies.

The message from the above analysis is twofold. First, it shows that the microwave parameters (permittivity, loss tangent) of the ferroelectric films (and varactors) may be predicted from relatively simple low frequency *I-V* and *C-V* measurements. Second, it shows that further improvement of the performance of the ferroelectric varactors (films) may be achieved by the reduction of the density of the oxygen vacancies. However, the density of the oxygen vacancies may be determined by the thermodynamic equilibrium associated with the film/interface internal strains. In this case, the study of the correlation of the microwave properties of the ferroelectric capacitors with the complex action of the interfacial strains and oxygen vacancies may help to eliminate/reduce the negative effects on the performance of the varactors. This requires a careful microstructural analysis of the ferroelectric film and interfacial layer. The results of such an analysis may help to select appropriate buffer layers and deposition conditions aimed at controllable monitoring of the interfacial strains and the density of the oxygen vacancies in the ferroelectric films.

ACKNOWLEDGMENTS

This work was supported by the Swedish Strategic Research Foundation SSF (Oxide program and HSEP Research Center) and VINNOVA (PIDEA/Pacific Boat).

[1]A. Tombak, J.-P. Maria, F. T. Ayguavives, Z. Jin, G. T. Stauf, A. I. Kingon, and A. Mortazawi, IEEE Trans. Microwave Theory Tech. **51**, 462 (2003).
[2]R. A. York, A. S. Nagra, P. Periaswamy, O. Auciello, S. K. Streiffer, and J. Im, Integr. Ferroelectr. **34**, 177 (2001).
[3]D. Kuylenstierna, G. Subramanyam, A. Vorobiev, and S. Gevorgian, Microwave Opt. Technol. Lett. **39**, 81 (2003).
[4]B. Acikel, T. R. Taylor, P. J. Hansen, J. S. Speck, and R. A. York, IEEE Microw. Wirel. Compon. Lett. **12**, 237 (2002).
[5]A. Vorobiev, P. Rundqvist, K. Khamchane, and S. Gevorgian, Appl. Phys. Lett. **83**, 3144 (2003).
[6]A. K. Tagantsev, V. O. Sherman, K. F. Astafiev, J. Venkatesh, and N. Setter, J. Electroceram. **11**, 5 (2003).
[7]O. G. Vendik, L. T. Ter-Martirosyan, and S. P. Zubko, J. Appl. Phys. **84**, 993 (1998).
[8]K. Jonscher, *Dielectric Relaxation in Solids* (Chelsea Dielectrics Press Ltd, London, 1983), pp. 87–89.
[9]O. G. Vendik and L. T. Ter-Martirosyan, J. Appl. Phys. **87**, 1435 (2000).
[10]P. Li and T.-M. Lu, Phys. Rev. B **43**, 14261 (1991).
[11]G. W. Dietz, W. Antpohler, M. Klee, and R. Waser, J. Appl. Phys. **78**, 6113 (1995).
[12]P. C. Joshi and S. B. Krupanidhi, J. Appl. Phys. **73**, 7627 (1993).
[13]M. S. Tsai and T. Y. Tseng, Mater. Chem. Phys. **57**, 47 (1998).
[14]C. A. Mead, Phys. Rev. **128**, 2088 (1962).
[15]K. Bethe, Philips Res. Rep., Suppl. **2**, 74 (1970).
[16]Alexander Tagantsev, Appl. Phys. Lett. **76**, 1182 (2000).
[17]O. G. Vendik and A. N. Rogachev, Tech. Phys. Lett. **25**, 702 (1999).
[18]A. Fraser, R. Ares, and R. Gleason, *Introduction to Bipolar Device GHz Measurement Techniques* (Cascade Microtech, Beaverton, 2003).
[19]Z. Ma, A. J. Becker, P. Polakos, H. Huggins, J. Pastalan, H. Wu, Y. H. Wong, and P. Mankiewich, IEEE Trans. Electron Devices **45**, 1811 (1998).
[20]J. Petzelt *et al.*, Phys. Rev. B **64**, 184111 (2001).
[21]O. G. Vendik and S. P. Zubko, J. Appl. Phys. **88**, 5343 (2000).
[22]S. K. Streiffer, C. Baceri, C. B. Parker, S. E. Lash, and A. I. Kingon, J. Appl. Phys. **86**, 4565 (1999).
[23]D. E. Kotecki *et al.*, IBM J. Res. Dev. **43**, 367 (1999).
[24]A. R. Krauss *et al.*, Integr. Ferroelectr. **32**, 121 (2001).
[25]J. Im, S. K. Streiffer, O. Auciello, and A. R. Krauss, Appl. Phys. Lett. **77**, 2593 (2000).
[26]H.-C. Li, W. Si, A. D. West, and X. X. Xi, Appl. Phys. Lett. **73**, 464 (1998).
[27]C. Zhou and D. M. Newns, J. Appl. Phys. **82**, 3081 (1997).
[28]C. Basceri, S. K. Streiffer, A. I. Kingon, and R. Waser, J. Appl. Phys. **82**, 2497 (1997).
[29]A. von Hippel, *Dielectrics and Waves* (Artech House, Boston, 1995), pp. 228–234.
[30]B. H. Moeckly and Y. Zhang, IEEE Trans. Appl. Supercond. **11**, 450 (2001).
[31]Y. Lemaitre, B. Marcilhac, D. Mansart, J. Siejka, and J.-C. Mage, Physica C **372-376**, 667 (2002).
[32]S. Gevorgian, *Surface Impedance of Silicon Substrates and Films* (Wiley, New York, 1998), pp. 433–440.
[33]S. Abadei, S. Gevorgian, C.-R. Cho, and A. Grishin, J. Appl. Phys. **91**, 2267 (2002).
[34]V. M. Fridkin, *Ferroelectric Semiconductors* (Consultants Bureau, New York, 1980).
[35]C. Hubert, J. Levy, A. C. Carter, W. Chang, S. W. Kirchoefer, J. S. Horwitz, and D. B. Chrisey, Appl. Phys. Lett. **71**, 3353 (1997).
[36]S. M. Sze, *Physics of Semiconductor Devices* (Wiley, New York, 1981), pp. 402–403.
[37]M. S. Tsai, S. C. Sun, and T.-Y. Tseng, IEEE Trans. Electron Devices **46**, 1829 (1999).
[38]Landolt-Börnstein, in *Numerical Data and Functional Relationship in Science and Technology*, edited by K.-H. Hellwege and A. M. Hellwege (Springer, Berlin, 1981), Vol. 16.
[39]W. A. Feil and B. W. Wessels, J. Appl. Phys. **74**, 3927 (1993).
[40]S. Saha and S. B. Krupanidhi, Appl. Phys. Lett. **79**, 111 (2001).
[41]N. D. Browning, H. O. Moltaji, and J. P. Buban, Phys. Rev. B **58**, 8289 (1998).
[42]J. Gerblinger and H. Meixner, J. Appl. Phys. **67**, 7453 (1990).
[43]M. J. Dalberth, R. E. Stauber, J. C. Price, C. T. Rogers, and D. Galt, Appl. Phys. Lett. **72**, 507 (1998).
[44]X. Zhu, J. Zhu, S. Zhou, Z. Liu, N. Ming, S. Lu, H. L.-W. Chan, and C-L Choy, J. Electron. Mater. **32**, 1125 (2003).
[45]M. Hiratani, K. Imagawa, and K. Takagi, J. Appl. Phys. **78**, 4258 (1995).
[46]L. A. Knauss, J. M. Pond, J. S. Horwitz, D. B. Chrisey, C. H. Mueller, and R. Treece, Appl. Phys. Lett. **69**, 25 (1996).
[47]C. Ang, R. Guo, A. S. Bhalla, and L. E. Cross, J. Appl. Phys. **87**, 3937 (2000).
[48]T. R. Taylor, P. J. Hansen, B. Acikel, N. Pervez, R. A. York, S. K. Streiffer, and J. S. Speck, Appl. Phys. Lett. **80**, 1978 (2002).
[49]W. Chang, J. S. Horwitz, A. C. Carter, J. M. Pond, S. W. Kirchoefer, C. M. Gilmore, and D. B. Chrisey, Appl. Phys. Lett. **74**, 1033 (1999).
[50]P. K. Petrov, Z. G. Ivanov, and S. S. Gevorgyan, Mater. Sci. Eng., A **288**, 231 (2000).
[51]N. A. Pertsev, A. G. Zembilgotov, S. Hoffman, R. Waser, and A. K. Tagantsev, J. Appl. Phys. **85**, 1698 (1999).
[52]Z.-G. Ban and S. P. Alpay, J. Appl. Phys. **91**, 9288 (2002).